Applied Physics A (2024) 130:445
https://doi.org/10.1007/s00339-024-07603-7

Neodymium (III)-containing poly(lactide-co-glycolide)-coated robocast bioactive glass scaffolds for photothermal therapy and bone regeneration

Aylin M. Deliormanlı[1]

Received: 19 January 2024 / Accepted: 19 May 2024 / Published online: 28 May 2024
© The Author(s) 2024

Abstract
In this study, trivalent neodymium-doped silicate-based 13–93 bioactive glass scaffolds were prepared by the robocasting method using sol-gel-derived bioactive glass powders for tissue engineering applications. Sintered scaffolds were coated by borate-based 13-93B3 bioactive glass-containing polylactide-co-glycolide solution. The produced composite scaffolds' mechanical, morphological, and structural characteristics were thoroughly examined, as their in vitro bioactivity in cell culture media and simulated body fluid. Furthermore, the scaffolds' amoxicillin adsorption and release behavior was examined over time. The outcomes demonstrated that it was feasible to effectively create periodic, mesh-like-patterned robocast glass scaffolds utilizing Nd^{3+}-doped sol-gel-derived bioactive glass powders. The scaffolds' compressive strengths ranged from 10.02 MPa to 18.6 MPa, with the PLGA-coated scaffolds exhibiting the highest strength values. All of the scaffolds that were submerged in simulated body fluid for 28 days showed hydroxyapatite formation. The presence of borate glass on the surface of the silicate-based glass scaffolds improved the hydroxyapatite formation ability. The quantity of drug adsorption for all types of scaffolds was measured to be between 4 and 9% whereas the cumulative drug release was in the range of 58 to 96%. Borate glass particle-containing PLGA coating enhanced the drug delivery behavior.

Keywords Bioactive glass · Neodymium · Robocasting · Scaffolds · PLGA · Amoxicillin

1 Introduction

Bioactive glasses have become multipurpose devices for orthopedic implant coatings, angiogenesis, soft and hard tissue engineering, and drug/growth factor delivery in recent years. They are characterized by remarkable attributes such as osteoconductivity, biocompatibility, and a regulated rate of disintegration. They also display antibacterial and angiogenic features [1–5]. Furthermore, bioactive glasses have a broad range of applications since they can incorporate different biologically active elements such as magnesium, zinc, strontium, and fluorine [5] as well as the ions of rare earth elements [6–9] or they can be utilized in the fabrication of bioactive polymer composites [10].

Currently, fluorescent biocompatible nanocrystals are known to hold substantial potential as contrasting agents for fluorescence imaging. These nanoparticles often display multifunctional capabilities, serving as nanoprobes for the diagnosis of malignant tumors at early stages and as therapeutically active compounds. Recent studies have focused on lanthanide-doped fluorescent nanocrystals and glasses for high-contrast in vitro and in vivo imaging and therapy [6–14].

Among the rare earth ions of the lanthanide group, neodymium (Nd^{3+}) possesses distinctive characteristics. Previous studies have reported the appropriate doping of nanocrystals and glasses with Nd^{3+} for obtaining fluorescent nanoprobes for photoluminescence tissue imaging. Additionally, Nd^{3+}'s spectroscopic characteristics have been reported as suitable for photothermal therapy as well as nanothermometry, and optical bioimaging applications [15–17].

✉ Aylin M. Deliormanlı
aylin.deliormanli@cbu.edu.tr

[1] Department of Metallurgical and Materials Engineering, Biomaterials Laboratory, Manisa Celal Bayar University, Yunusemre, Manisa, Turkey

Neodymium as a rare earth element holds significant importance in laser physics [18]. When incorporated as a trivalent dopant ion, neodymium (Nd^{3+}, [Xe] $4f^3$) ion exhibits unique features. For example, under the stimulation of an 808-nm laser, Nd^{3+} ions generate thermal energy as well as emit light (infrared fluorescence), making them suitable for the fabrication of multi-functional materials having photothermal and photoluminescence thermometry features [15, 19]. Previous research has shown the suitability of nanocrystals and glasses doped with Nd^{3+} and other metal oxides for obtaining fluorescent nanoprobes for deep tissue bioimaging, as well as their use in photothermal therapy [20], and nanothermometry [21, 22].

A study conducted by Yusof and colleagues [23] involved the preparation of P_2O_5-MgO-$ZnSO_4$-based glasses using the melt-quenching method, with the substitution of neodymium ions at different concentrations. The incorporation of neodymium ions into the glass structure enhanced its light absorption behaviour and physical properties, potentially enabling its use in photonic devices like infrared solid-state lasers.

Another study by Yu et al. [24] reported neodymium to be ideal for in vivo fluorescence imaging. The results of the study suggested that Nd^{3+}-doped CaF_2 nanoparticles could be utilized as imaging probes for in vitro photoacoustic imaging, in addition to fluorescence and magnetic resonance imaging. Consequently, neodymium-doped nanoparticles have shown high potential in biomedical applications because of their biocompatibility and suitability as multimodal imaging sensors.

Rehman and colleagues' study [25] demonstrated that cobalt-ferrite nanoparticles containing neodymium exhibited high magnetic and antimicrobial properties. This study highlighted the significant potential of neodymium-containing cobalt-ferrite nanoparticles in pharmaceutical and biomedical applications.

El-Bashir and colleagues [26] produced silica-titania-based glass monoliths with various percentages of neodymium ions using the sol-gel technique. The structural characteristics of the glasses were investigated through X-ray diffraction analysis, confirming their amorphous nature. Photo-capacitance and photo-resistance properties were examined in a frequency range (20 Hz-3 MHz) at 25 °C and under different illumination intensities. The results indicated the potential use of these synthesized glasses in optoelectronic applications like photo-resistant and photo-capacitive sensors [26].

Ma and colleagues [27] studied the synthesis of bioactive Nd_2O_3-CaO-SiO_2 glasses to be utilized in photoluminescence thermometry, photothermal therapy (PTT), and burned tissue repair. Injectable gels were obtained by mixing Nd_2O_3-CaO-SiO_2 bioactive glasses with sodium alginate solution. The results suggested that such multifunctional biomaterials could not only serve as implantable agents and tissue repair functions for PTT-based cancer treatment but also act as materials for temperature monitoring to be utilized in localized temperature measurements.

While previous studies in the field have mainly focused on the optical properties of ceramics and glasses containing Nd^{3+} for deep tissue fluorescence imaging, there are only few articles addressing the biomedical applications of this relevant rare earth element ion. Furthermore, to the best of the authors knowledge there is no published study on the fabrication of SiO_2-based 13–93 bioactive glasses containing Nd^{3+}. Therefore, the main goal of the current study was to prepare Nd^{3+}-containing silicate-based bioactive glass scaffolds using the robocasting method and coat their surface with a polylactide-co-glycolide (PLGA) layer containing borate-based 13-93B3 bioactive glass particles. In the study, it was intended to investigate the structural, morphological, and mechanical properties as well as the bioactivity, and antimicrobial drug (amoxicillin) delivery behavior of the manufactured composite scaffolds. Besides the addition of Nd^{3+} into the silicate glass network, the use of two different bioactive glass compositions (SiO_2 and B_2O_3-based) in the same scaffold design is the novelty of the study. Through this approach higher bioactivity but lower chemical and mechanical strength of the 13-93B3 borate glass [4] compared to 13–93 glass can be compensated by the use of silicate glass in the core and the borate glass in the coating layer.

2 Experimental work

2.1 Material synthesis

Bioactive glass particles (BG) doped with Nd^{3+} in the composition of 13–93 (53 SiO_{2-x}, 6 Na_2O, 12 K_2O, 5 MgO, 20 CaO, 4 P_2O_5 wt%, where x = 0.5, 1, 3, 5 wt% Nd_2O_3), (see Table 1) were synthesized through the sol-gel method. The employed synthesis process was extensively detailed in previous studies [11, 28]. Initially, tetraethyl orthosilicate was combined with an aqueous nitric acid solution at room temperature, causing hydrolysis reaction, followed by agitation for 60 min. Afterwards, a sequence of other chemicals including triethyl phosphate, calcium nitrate tetrahydrate, sodium nitrate, magnesium nitrate hexahydrate, and potassium nitrate was added incrementally over 30 min. To the 13–93 bioactive glass solution, predetermined quantities of neodymium (III) acetate hydrate ($(CH_3CO_2)_3Nd{\cdot}xH_2O$, M_w: 321.37) were introduced. The obtained transparent solution was subjected to overnight agitation and then maintained at 25 °C within a sealed container to allow gel formation.

Table 1 Composition (wt%) of the bare and Nd^{3+}-containing silicate based 13–93 glasses prepared in the study

Code	SiO_2	CaO	Na_2O	K_2O	MgO	P_2O_5	Nd_2O_3
BG	53	20	6	12	5	4	-
0.5Nd-BG	52.5	20	6	12	5	4	0.5
1Nd-BG	52	20	6	12	5	4	1
3Nd-BG	50	20	6	12	5	4	3
5Nd-BG	48	20	6	12	5	4	5

Following gelation, it was aged at 60 °C for 48 h, followed by drying at 120 °C for 24 h. Subsequently, a heat treatment at 625 °C for 4 h with a heating rate of 5 °C/min was employed to eliminate residual organic components and decomposition of nitrates. The resulting calcined powders underwent a 10-minute grinding (at 700 rpm) process using a planetary ball mill (Fritch Pulverisette 7 Premium Line, Germany). All chemicals utilized in glass synthesis were high purity, bio-grade, and obtained from Sigma-Aldrich, Germany.

2.2 Scaffold preparation

Sol-gel-derived amorphous silicate 13–93 bioactive glass powders (median particle size was in the range of 5–6 μm) were used to fabricate 3D-bioactive glass scaffolds with periodic grid-like structures through the use of the robocasting technique (Fisnar NV 7400 N, USA). Using a magnetic stirrer, an aqueous Pluronic F-127 (Sigma- Aldrich) solution (25 wt%) was prepared at room temperature, and the polymer solution was then stored in a refrigerator at +4 °C. Next, to make the printing ink for robocasting, Nd^{3+}-doped sol-gel-derived bioactive glass powders (35 wt%) were combined with the F-127 solution [29]. Subsequently, the mixture was homogenized by spinning a planetary mixer (Uni-Cyclone UM-113, Japan) for 5 min at 1000 rpm. Any additional dispersant, like polyacrylic acid (PAA) or another kind of block-copolymer [30], which is frequently employed to stabilize inorganic particles in liquid-based systems, was not used because the resulting suspension was well-dispersed. Periodic, 1 cm-diameter porous scaffolds were printed at 25 °C with a dispenser-attached steel nozzle (d: 510 μm). Both the cylindrical and disc-shaped structures were designed to have a pore width of 1000 μm between the centers of the two rods (x-y-direction). The scaffolds were sintered for an hour at 675 °C after drying at room temperature.

For the preparation of polymer and borate glass-coated composites sintered scaffolds were immersed in a poly-lactide-co-glycolide (PLGA, lactide: glycolide 50:50, M_w 45.000 g/mol, Sigma Aldrich, Germany)-dichloromethane solution (5 wt%) containing melt-derived borate 13-93B3 bioactive glass (B_2O_3 56.6%, CaO 18.5%, Na_2O 5.5%, MgO 4.6%, K_2O 11.1%, P_2O_5 3.7% (wt%) particles (10 wt%) for 30 min while mixing by a magnetic stirrer. Before the coating process, borate 13-93B3 glass particle-containing PLGA solution was stirred for 30 min and further homogenized using an ultrasonic probe (Bandelin Sono-Puls, Germany) for 5 min. Coated scaffolds were dried at room temperature for 24 h before characterizations. For the synthesis of the 13-93B3 borate glass particles a platinum crucible was utilized and melting was made at 1100 °C for 1 h. The glass melt was quenched between cold steel plates. The size reduction was performed using a planetary ball mill [13]. Fig. 1 demonstrates the scaffold preparation procedure followed in the study.

2.3 Structural, morphological, mechanical characterizations

The characterization of the prepared bioactive glasses involved a combination of techniques. A Fourier transform infrared spectrometer (FTIR, Thermo Nicolet IS20, USA) was utilized in conjunction with an ATR accessory for molecular analysis. XRD was used to investigate the crystalline phase formation using a Malvern Panalytical X-ray diffractometer (CuKα radiation, scanning range 10–90°). The particle size distribution of the silicate and borate-based glass powders was obtained using a Malvern Mastersizer 3000 size analyzer.

To investigate the morphology of the prepared bioactive glasses, which were in the form of particles, scanning electron microscopy (SEM) using a Zeiss Gemini 500 instrument was employed. Morphology of the fabricated scaffolds was investigated using an optical microscope (Nikon, Japan). The surface of the glass samples was coated by Au/Pd using a sputter coater before SEM analysis.

The compressive strength of the manufactured bioactive glass layered cylindrical scaffolds (diameter: 7 mm and height: 8–9 mm) was tested using a mechanical compression testing device (Shimadzu, Japan) with a deformation rate of 0.5 mm/min. Five samples in each group were tested, and the data were expressed as a mean ± standard deviation. Before mechanical testing, any treatment such as grinding or polishing was not applied to the surface of the scaffolds. The load was applied in the direction perpendicular to the plane of deposition of the constructs.

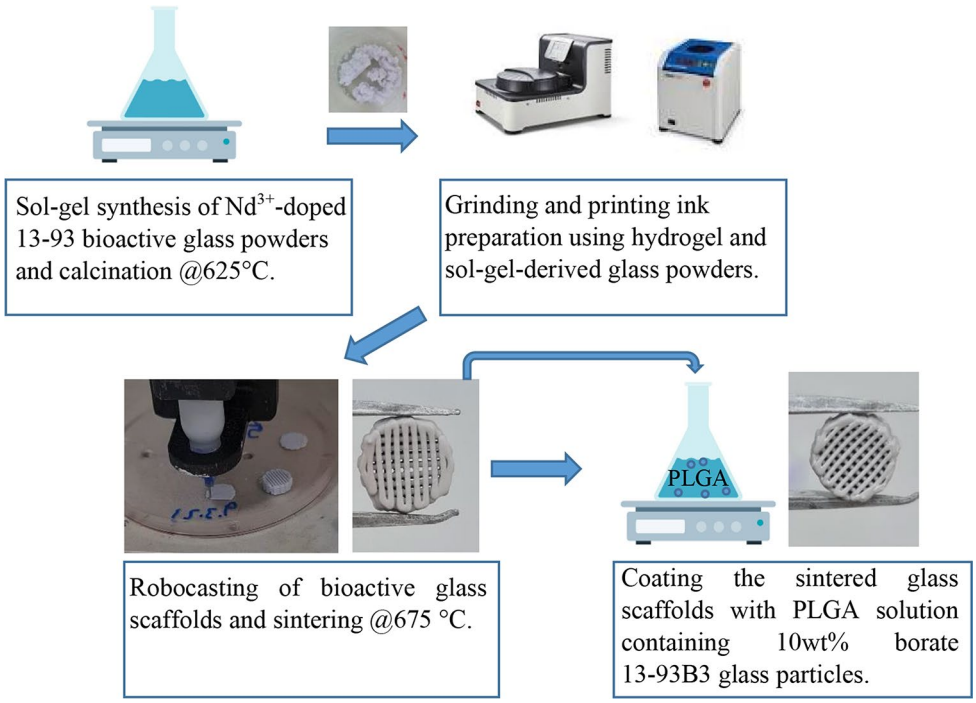

Fig. 1 Schematic of the PLGA-coated bioactive glass-based composite scaffold preparation procedure followed in the study

2.4 In vitro hydroxyapatite formation

The formation of the hydroxyapatite (HA) on the fabricated glass scaffolds was examined in simulated body fluid (SBF) and the minimum essential medium (α-MEM, Product no: M0644, Sigma-Aldrich, Germany) at 37 °C under static conditions. The simulated body fluid was prepared following the method reported by Kokubo et al. [31], involving the use of NaCl (M_w:58.44), $NaHCO_3$ (M_w:84.01), KCl, $K_2HPO_4.3H_2O$, $MgCl_2.6H_2O$, $CaCl_2$, Na_2SO_4, and $NH_2C(CH_2OH)_3$ (M_w:121.14), (all chemicals from Sigma-Aldrich, Germany). On the other hand, α-MEM is a mammalian cell culture media that contains inorganic as well as biological organic components of blood plasma [32].

For 7, 14, and 28 days, the bioactive glass scaffolds were cultured in an incubator after being immersed in SBF or α-MEM at an initial pH of 7.4 (1 gram of sample per 500 milliliters of SBF or α-MEM). They were then removed from the physiological fluids, dried at 60 °C. Using SEM and FTIR spectrometer, the presence of hydroxyapatite on the surfaces of the SBF or α-MEM-treated samples was assessed under predetermined parameters.

2.5 Drug loading and delivery studies

Amoxicillin (Sigma-Aldrich) was chosen as the drug model in the experimental studies to be carried out. Amoxicillin, a semisynthetic penicillin group antibiotic that can be used in the treatment of osteomyelitis (bone tissue infection), can be dissolved in water-based systems [33–35]. It has been reported that amoxicillin exhibits strong antibacterial activity against test bacteria, most of which are pathogenic and include Gram (-) and (+) bacteria [36]. For the drug loading experiments, 10 ml of drug solution (1 mg/ml) was mixed with each glass scaffold for 24 h at 25 °C. To determine the concentration and amount of drug adsorbed onto the bioactive glass samples, a UV-Vis spectrophotometer has been used at 270 nm (Thermo Fisher Scientific, Evolution 201, USA). Once the bioactive glass scaffolds were removed from the drug solution, they were dried for 48 h at 40 °C. For drug release testing, samples with known weights and loaded drug amounts were kept in phosphate-buffered saline (pH 7.4) solution at 37 °C. 2 ml sample was taken, and until the drug release plateau was reached, it was changed with a fresh 2 ml solution to check for any burst effects. Samples were taken at specified time intervals (hourly for the first 24 h and up to 360 h), and absorbance values at 270 nm were recorded using the UV-Vis spectrophotometer.

Drug release kinetics were studied using four different mathematical models namely zero-order, first-order, Higuchi, and Korsmeyer-Peppas models [37].

2.6 Statistical analysis

The one-way ANOVA followed by Tukey's post hoc test was performed. The p-value < 0.05 (*) or 0.01 (**) and 0.001 (***) were considered significant.

3 Results and discussion

Structural and morphological properties of the synthesized silicate and borate-based bioactive glass particles are given in Fig. 2 (a-j). Based on the XRD analysis results both 13–93 (Fig. 2c) and 13-93B3 (Fig. 2f) bioactive glass particles were amorphous. The synthesized silicate-based bioactive glass powders have a wide particle size distribution and the Nd^{3+} addition did not cause a significant change in the particle morphology. According to the results of the measurements performed with the particle size analyzer, the d_{50} particle size of the bare and the Nd^{3+}-doped silicate glass powders was between 5 and 6 µm. SEM micrograph of the 0.5%Nd^{3+}-containing bioactive glass powders also demonstrates the existence of particles smaller than 1 µm. On the other hand, the median particle size of the melt-derived 13-93B3 glass powders was 2.5 µm and the FTIR spectrum of the related powder contains bands representing the vibrational stretching of triangular BO_3 and tetrahedral BO_4 groups [38]. Fig. 2 (h) and (i) also demonstrate the digital images of the robocast composite scaffolds prepared in the study. XRD pattern of the sintered scaffolds given in Fig. 2 (j) indicates the amorphous structure was kept after heat treatment at 675 °C.

Optical micrographs of the uncoated Nd^{3+}-containing silicate-based bioactive glass disc-shaped scaffolds are shown in Fig. 3. Based on the images scaffolds (diameter ~ 7 mm, height ~ 5 mm) have interconnected porosity with oriented pore structure. The homogeneous, interconnected porous network produced by the robocasting method may enhance the adhesion, viability, and proliferation of the cells [39] when the scaffolds are implanted into the body. Results also showed that the inclusion of the Nd^{3+} in the glass network did not cause a change in the morphology of the fabricated scaffolds. The strut diameter of the periodic scaffolds was measured to be in the range of 400 µm to 475 µm. The porosity of the prepared scaffolds was calculated to be 65–70% based on the measurement of the weight

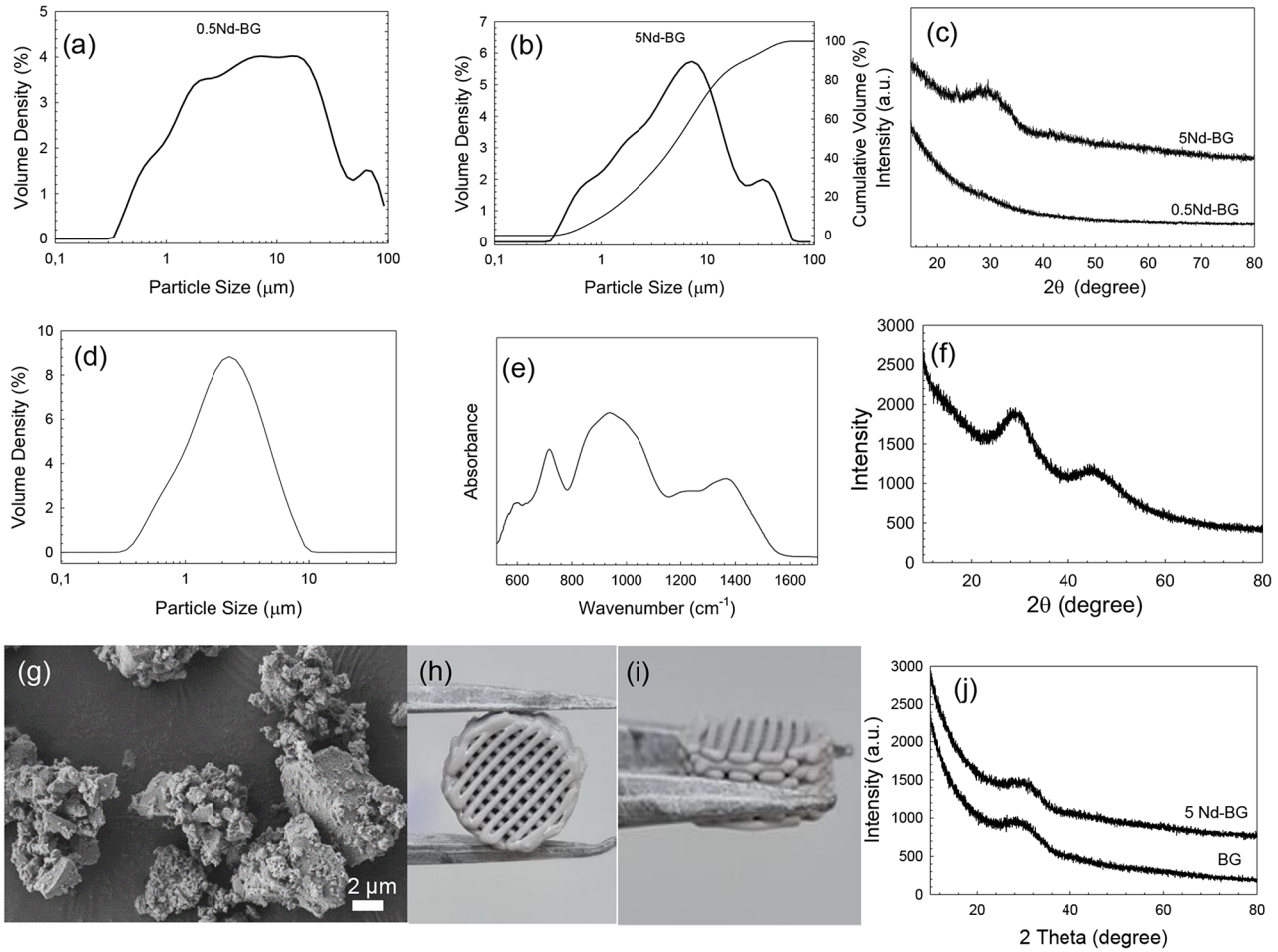

Fig. 2 (**a**), (**b**) Particle size distribution graphs, and (**c**) XRD pattern of the sol-gel-derived silicate-based 0.5Nd-BG and 5Nd-BG bioactive glass powders; (**d**) particle size distribution graph, (**e**) FTIR spectrum, (**f**) XRD pattern of the melt-derived borate-based 13-93B3 bioactive glass powders; (**g**) SEM micrograph of the 5Nd-BG bioactive glass particles calcined at 625 °C and (**h**), (**i**) digital images and (**j**) XRD pattern of robocast bioactive glass scaffolds fabricated using bare and 5Nd-BG glass powders

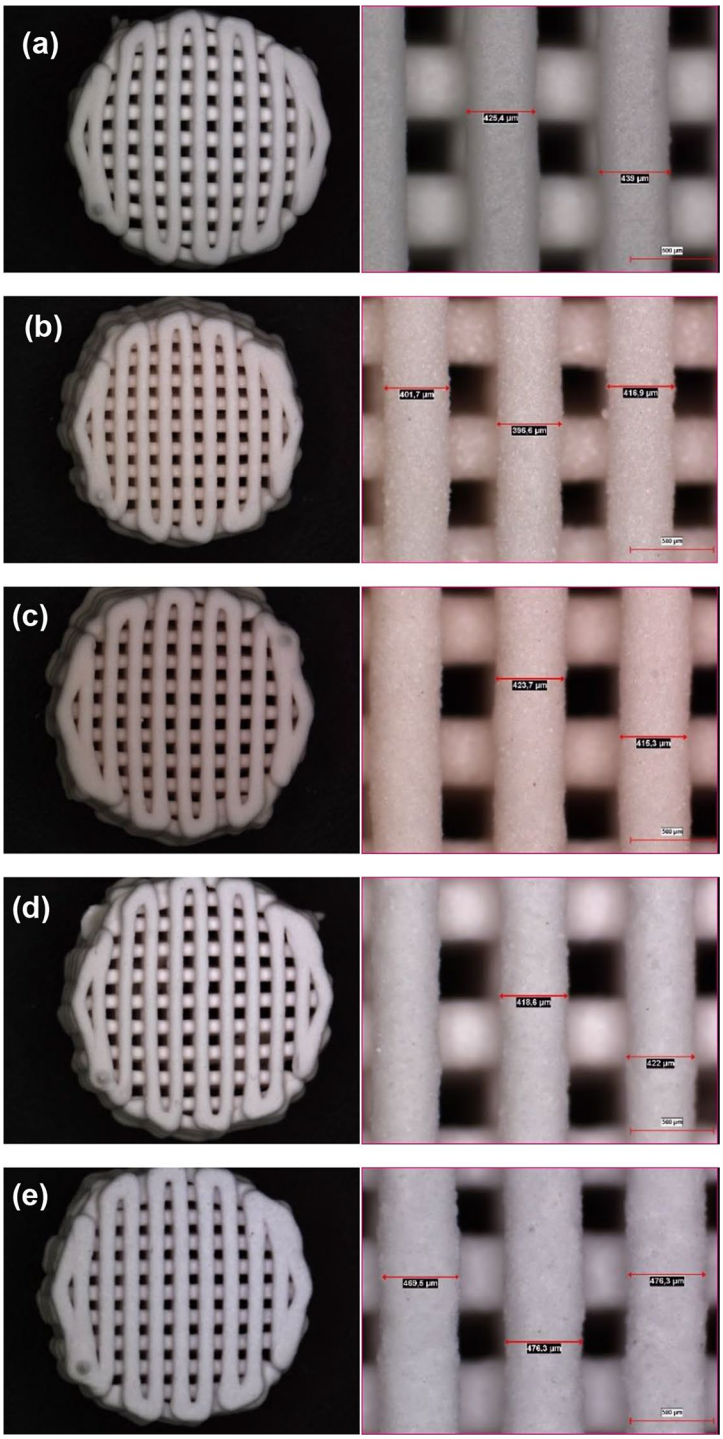

Fig. 3 Optical microscope images of the (**a**) bare, (**b**) 0.5 Nd^{3+}, (**c**) $1Nd^{3+}$, (**d**) $3Nd^{3+}$, (**e**) $5Nd^{3+}$-containing silicate 13–93 bioactive glass scaffolds. Scale bar: 500 µm

and the dimensions. Similarly, optical microscope images of the 13-93B3 glass particle-containing PLGA-coated bioactive glass composite scaffolds are demonstrated in Fig. 4. Accordingly, the presence of borate glass powders and a polymer coating layer did not cause a significant difference in the scaffold morphology. Any clogging problem was not observed due to the use of low polymer concentration during the coating process. Results also revealed that the presence of a coating layer did not cause a decrease in the total porosity of the composite scaffolds.

FTIR spectra of the uncoated and polymer-coated (in the presence of borate glass) Nd^{3+}-doped silicate bioactive glass scaffolds are shown in Fig. 5. FTIR spectra of the fabricated bioactive glass scaffolds demonstrated the existence of the Si-O vibration bands. In particular, the band at about ~ 790 cm^{-1} is the indication of symmetric

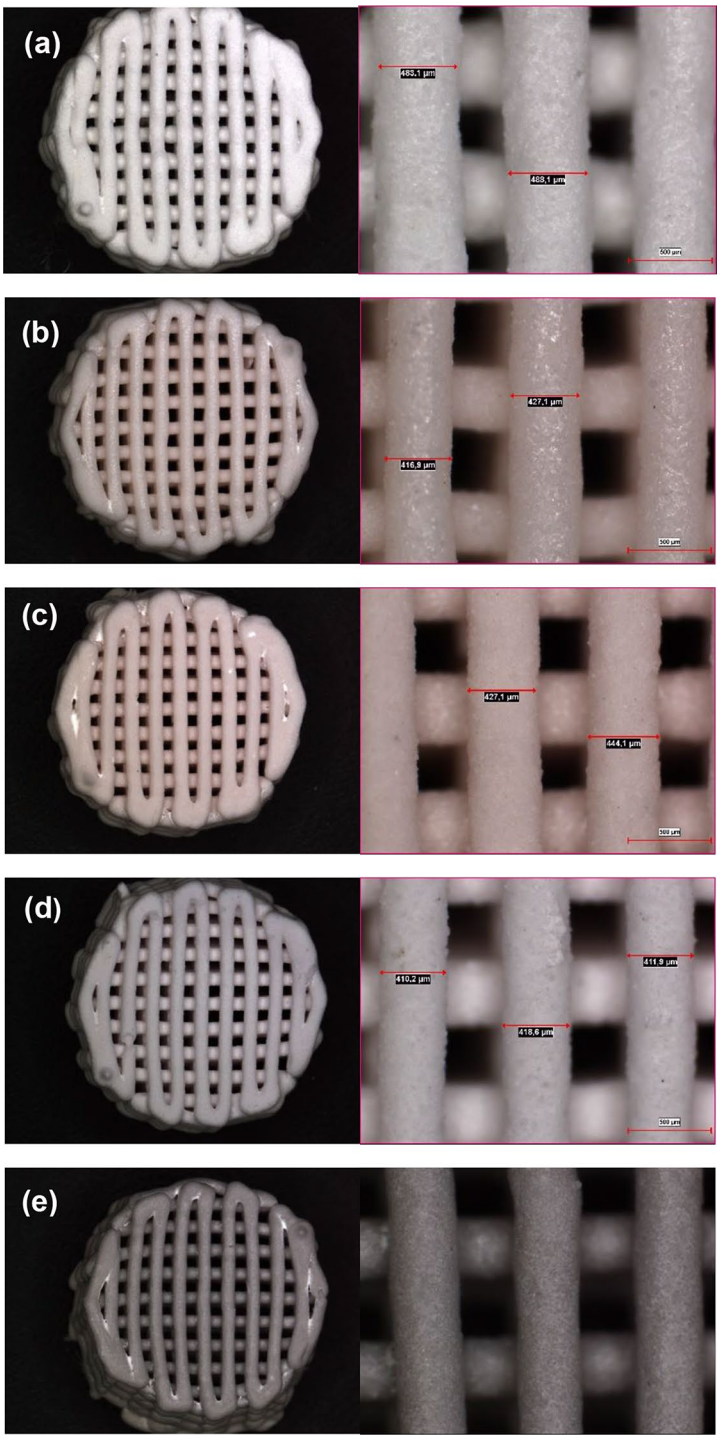

Fig. 4 Optical microscope images of the (**a**) bare, (**b**) 0.5 Nd^{3+}, (**c**) $1Nd^{3+}$, (**d**) $3Nd^{3+}$, (**e**) $5Nd^{3+}$-containing silicate 13–93 bioactive glass scaffolds after coating with PLGA in the presence of 10 wt% borate 13-93B3 glass particles. Scale bar: 500 µm

stretching in the Si-O-Si plane, which is the vertical movement of oxygen atoms. Furthermore, the more prominent band in the 980–1100 cm^{-1} region is associated with asymmetric stretching of Si–O–Si, i.e., horizontal movement of oxygen atoms inside the Si–O–Si plane [40, 41]. The weak band observed in the spectra at ~1350 to 1400 cm^{-1} can be explained by the presence of NO_3^- ions [42]. .

Results also showed that the FTIR spectra of the uncoated bioactive glass scaffolds (Fig. 5a) and the Nd^{3+}-containing silicate glass particles synthesized through the sol-gel process were similar. This indicates that the sintering process at 675 °C does not change the amorphous structure of the scaffolds and does not cause crystallization. The FTIR spectra of PLGA-coated scaffolds containing borate-based 13-93B3 BG powders are similar and no peak belonging to PLGA

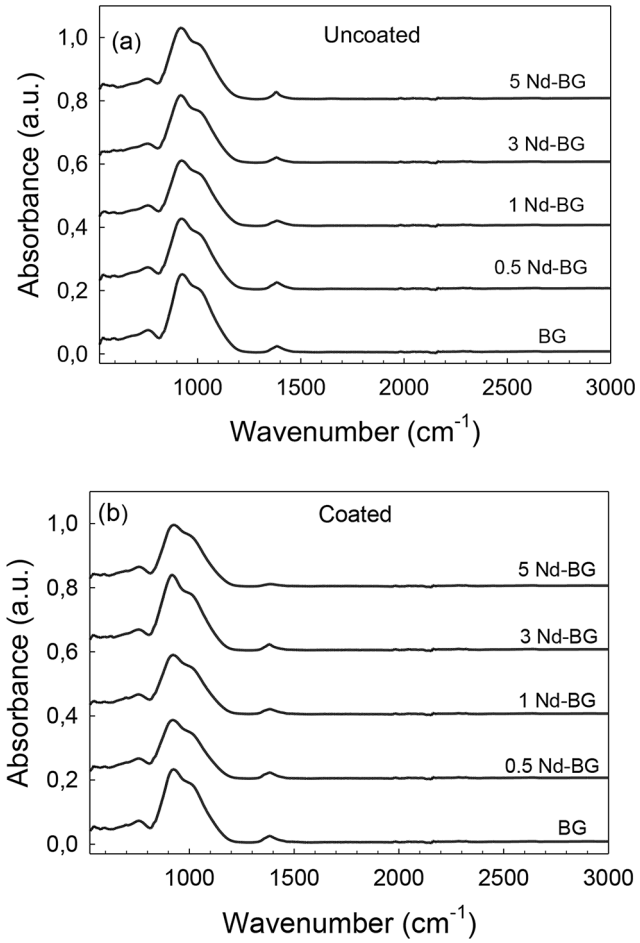

Fig. 5 FTIR spectra of the Nd^{3+}-doped 13–93 bioactive glass scaffolds (**a**) uncoated and (**b**) borate 13-93B3 glass-containing PLGA-coated

was detected in the structure which is presumably due to the low concentration of the polymer solution (5 wt%) utilized. In addition, the amorphous structure of borate-based bioactive glass powders and the fact that they were used in relatively low concentration caused the relevant samples to not be included in the FTIR spectra. Another reason for the absence of borate-based bioactive glass and PLGA coating in the spectra is that as they are applied only on the surface. For FTIR analysis, all of the scaffolds were ground using an agate mortar, and a very small amount of sample was used for the FTIR analysis. The fact that the sample taken comes from the inner parts of the scaffolds may be the reason for the absence of the related groups in the IR spectrum.

In the study compressive strength of the fabricated uncoated and polymer-coated scaffolds were measured under the same conditions and results are shown in Fig. 6. Accordingly, while the compressive strength of bare 13–93 bioactive glass scaffolds without any coating was measured as 10.02 MPa, this value was obtained as 17.25 MPa for the PLGA-coated sample containing borate glass particles. The force vs. stroke graphs of the as-fabricated uncoated and coated scaffolds in compression is shown in Fig. 6 (b) and (c). When compared to the uncoated glass scaffold alone, the peak load increased by ~84% in the case of coated 13–93 scaffolds (with a max. strain of 9.15%). The multi-peak trend may be attributed to the multiple fracture events that occurred during the compression test.

Results revealed that the addition of Nd^{3+} to the silicate glass network structure also affected the mechanical properties. The compressive strength of 3% Nd^{3+}-containing bioactive scaffolds was measured to be ~15 MPa, and it was understood that the compressive strength increased to 18.57 MPa by coating the same scaffolds with PLGA containing 13-93B3 bioactive glass powders. The compressive strength of the fabricated scaffolds was sufficient to use in tissue engineering applications such as the repair of trabecular bone defects [43]. It was previously reported that the compressive strength of PLGA/calcium silicate scaffolds was significantly improved compared to uncoated calcium silicate scaffolds [44]. A past study by Deliormanlı et al. [45] showed that PLGA-coated borate glass scaffolds have higher compressive strength compared to uncoated or PCL-coated glass scaffolds. Kang et al. [46] reported that the infiltration of PLGA improved the compressive strength (from 2.90 to 4.19 MPa), bending strength (from 1.46 to 2.41 MPa), and toughness (from 0.17 to 1.44 MPa) of beta-tricalcium phosphate scaffolds. These improvements obtained in the mechanical properties were attributed to the combination of the systematic coating of struts, and crack bridging.

FTIR spectra of the fabricated uncoated, Nd^{3+}-doped silicate-based bioactive glass scaffolds after immersion in alpha-MEM for 3 and 7 days are shown in Fig. 7. Similarly, the FTIR spectra of the same type of scaffolds soaked in simulated body fluid for 7, 14 and 28 days are shown in Fig. 8. The IR spectra of the bioactive glass scaffolds containing Nd^{3+} treated in SBF for 7 days showed doublet peaks at 603 cm^{-1} and 556 cm^{-1}, as well as a broad band at about 1035 cm^{-1}. The v_3 bending mode of $PO_4^{3-}$is shown by the ~1035 cm^{-1} band. The v_1 mode of PO_4^{3-} is indicated by the small peak at 961 cm^{-1}. The v_4 P-O bending of PO_4^{3-} is indicated by the peaks at ~556 cm^{-1} and 603 cm^{-1}, which suggest the presence of orthophosphate lattices [47, 48]. The asymmetric stretching (v_3) and out-of-plane bending (v_2) vibrations are responsible for the peaks at around 1390 cm^{-1} and 881 cm^{-1}, respectively. This suggests that carbonates have formed on the glass surface. The peak at around 1480 cm^{-1} represents the v_1 stretching modes of CO_3^{2-} [49]. Findings of the mineralization experiments also indicated that as the soaking time in SBF was extended an increment in absorption band intensities was recorded. Samples treated in simulated body fluid for 28 days have the highest intensities of bands at 556 cm^{-1} and

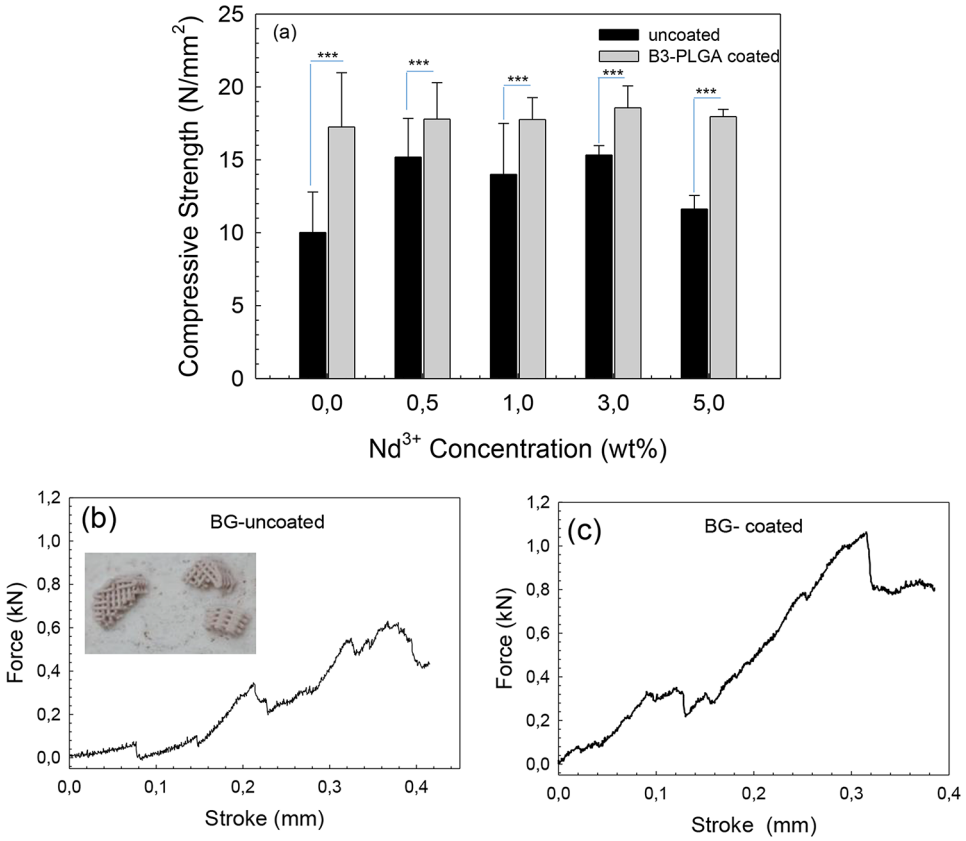

Fig. 6 (**a**) Graph showing the compressive strength of the fabricated bioactive scaffolds; Force vs. stroke graphs of the (**b**) uncoated, (**c**) coated bare 13–93 glass scaffolds

603 cm^{-1} representing crystalline HA formation. Additionally, absorbance intensities were lower for bioactive glass samples treated in α-MEM compared to the samples that were immersed in SBF for the same amount of time. The medium utilized in bioactivity experiments contains L-glutamine, ribonucleosides, and deoxyribonucleosides, without sodium bicarbonate, and is suitable for cell culture. Some complex solutions that are utilized for cell culture studies were also used in acellular bioactivity experiments previously for bioactive glasses [50]. For example, Sepulveda et al. [51] investigated the dissolution behavior of 45S5 bioactive glass powders in SBF and α-MEM culture medium. FTIR, XRD, and SEM evaluation of surface alterations demonstrated a decrease in HA formation in the α -MEM. This result was attributed to the presence of proteins in the cell culture medium that are missing in SBF. It was reported that the proteins formed a coating layer because their charge attracted the negative surface charge of the glass. By creating a barrier between the glass and the aqueous media, this coating subsequently prevents the glass from breaking down. On the other hand, because this barrier is permeable, silica and other ionic species can dissolve through it more slowly [51].

FTIR spectra of the PLGA-coated scaffolds after contact with the SBF for different periods are shown in Fig. 9. The same bands representing the formation of crystalline HA were observed in the spectra starting from the 7 days of immersion. FTIR analysis results also revealed that the inclusion of the Nd^{3+} ions (up to 3 wt%) to the bioactive glass network did not cause a detrimental influence on the HA formation ability in SBF for both uncoated and coated composite scaffolds. In addition, after 28 days of immersion in SBF bioactivity of the borate glass particle-containing PLGA-coated silicate glass scaffolds was higher compared to the uncoated glass samples. This may be attributed to the presence of 13-93B3 borate glass which is more bioactive compared to the silicate-based counterparts on the surface of the scaffolds due to its low chemical durability and fast dissolution rates when immersed in SBF or other physiological fluids [4, 52, 53].

The SEM micrographs of the borate glass particle-containing PLGA-coated 13-93 glass scaffolds after immersion in SBF for 28 days are shown in Fig. 10. Micrographs show the presence of the partial PLGA layer on the surface of the glass scaffolds after 28 days' contact with the SBF. Accordingly, the surface of the 0.5% and 5%Nd^{3+}-containing glass composite scaffolds was also covered with the hydroxyapatite particles. The plate-like morphology of the second-phase material observed on the surface of the samples was consistent with the morphology of crystalline hydroxyapatite [54].

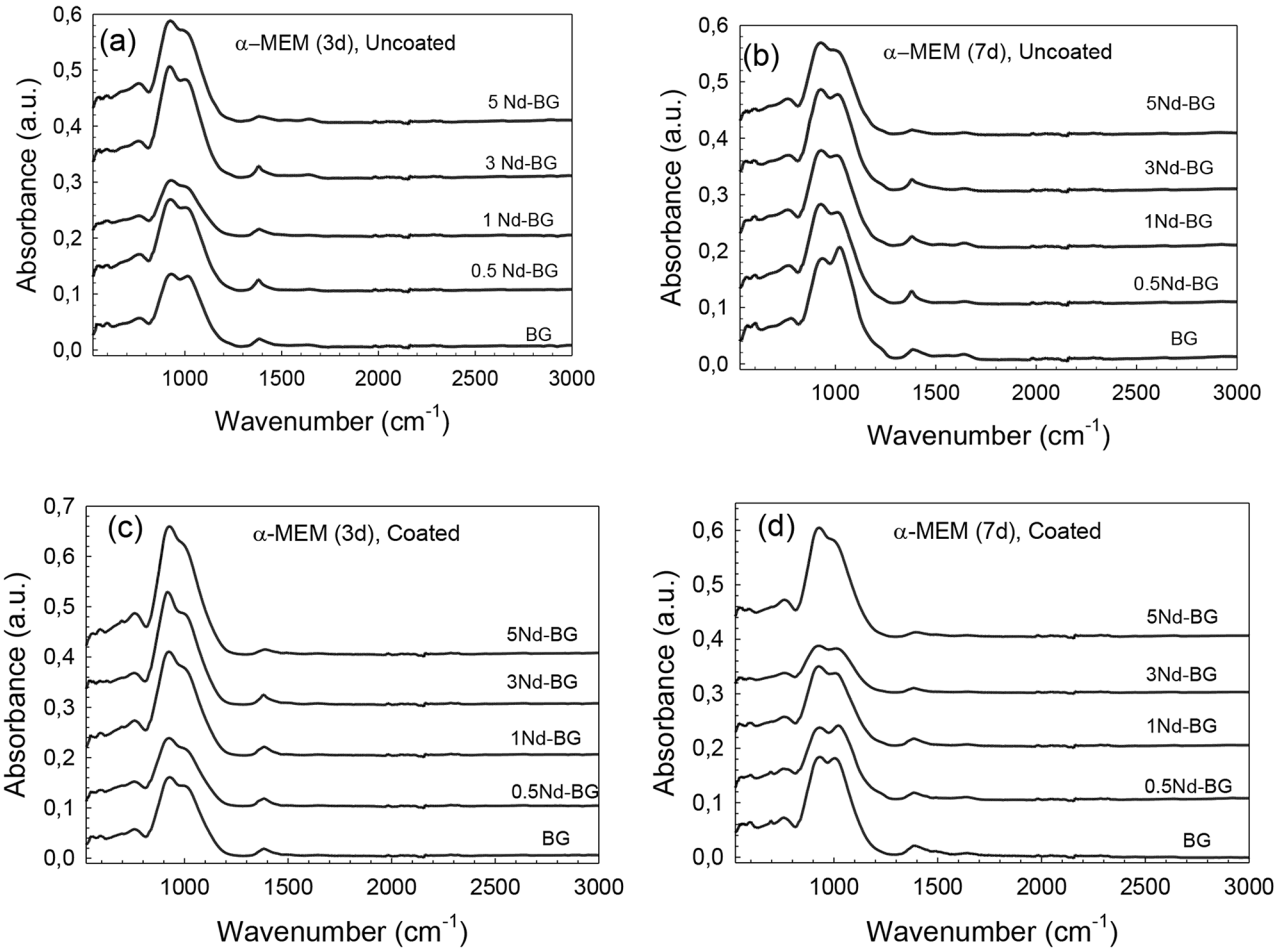

Fig. 7 FTIR spectra of the Nd^{3+}-containing (**a**), (**b**) uncoated, (**c**), (**d**) borate glass-containing polymer- coated bioactive glass scaffolds immersed in α-MEM for 3 days, and 7 days

Figure 11 demonstrates the aqueous AMOX solution (1 mg/ml) adsorption percentages to the bioactive glass scaffolds fabricated in the study. Accordingly, the drug adsorption percentage of the uncoated bioactive glass scaffolds (4–6%) was slightly lower compared to the borate glass particle-containing PLGA-coated silicate glass scaffolds (7–9%). Low drug adsorption percentages obtained may be attributed to the negative surface charge of bioactive glass scaffolds due to the presence of hydroxide (OH) groups on their surface [55]. The negatively charged glass scaffold surface may be considered the main difficulty in loading negatively charged amoxicillin. Cumulative drug release percentages shown in Fig. 12 indicated that the AMOX release amounts of the polymer-coated bioactive glass scaffolds were higher compared to the uncoated glass scaffolds. After 360 h, the cumulative drug release amount to the PBS medium was calculated to be 96% for the polymer-coated 5% Nd^{3+}-containing glass scaffolds. Under the same conditions, the drug release percentage was 76% in the absence of coating. Results also showed that an increase in the drug release rates was obtained as the Nd^{3+} concentration was increased. A higher drug release obtained for the PLGA-coated scaffolds may be attributed to the presence of the 13-93B3 bioactive glass particles in the polymer matrix. The higher reactivity of the borate glass particles in an aqueous medium compared to the silicate-based bioactive glass scaffolds may accelerate the dissolution of the amoxicillin into the PBS. Previously, Tibia et al. [56] performed amino-functionalization for aqueous amoxicillin solution (4 mg/ml) loading, to the mesoporous bioactive glass nanoparticles to obtain high drug loading efficiencies (~50%).

The drug release kinetics were studied by fitting the drug release data with zero-order, first-order, Higuchi, and Korsmeyer-Peppas mathematical models. Tables 2 and 3 show the model parameters (K) and coefficient of regression (R^2) values obtained from the model equations for the uncoated and coated-glass scaffolds, respectively. It was found that the drug delivery from the scaffolds was in accordance with the Higuchi model (the highest regression coefficient, R^2, was obtained in this model). After the Higuchi kinetic

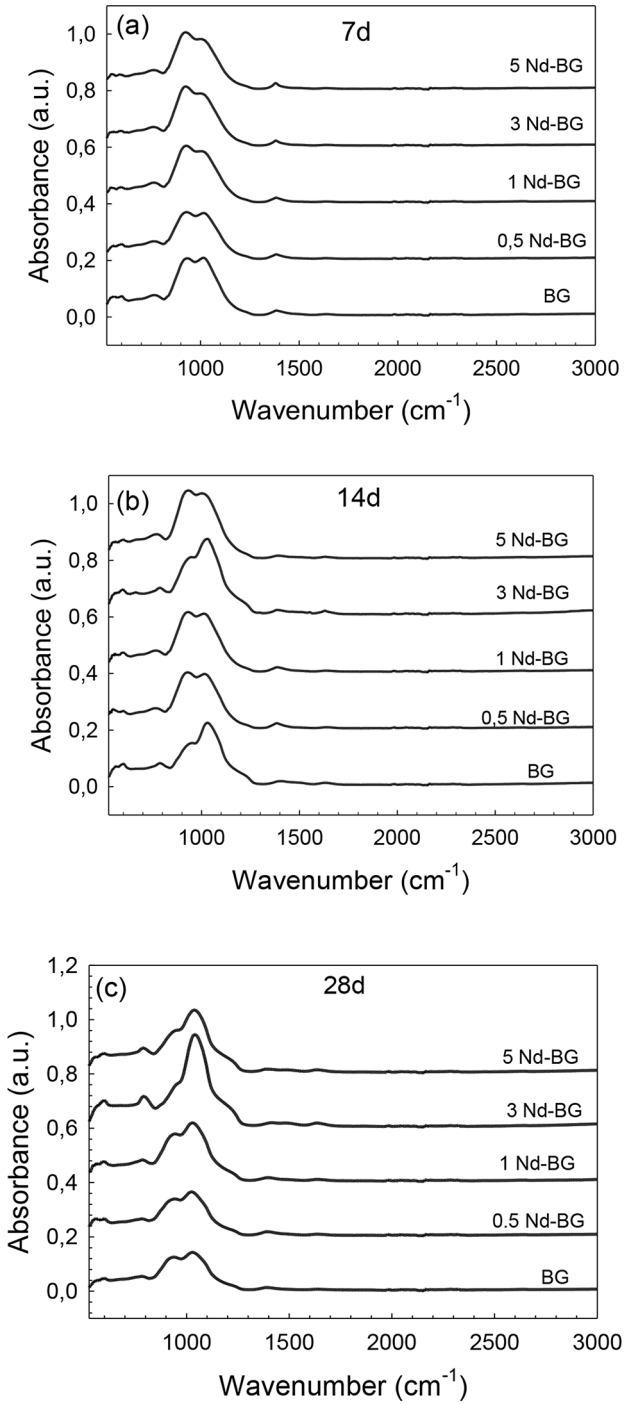

Fig. 8 FTIR spectra of the uncoated Nd^{3+}-containing 13–93 bioactive glass scaffolds immersed in SBF for (**a**) 7, (**b**) 14, and (**b**) 28 days

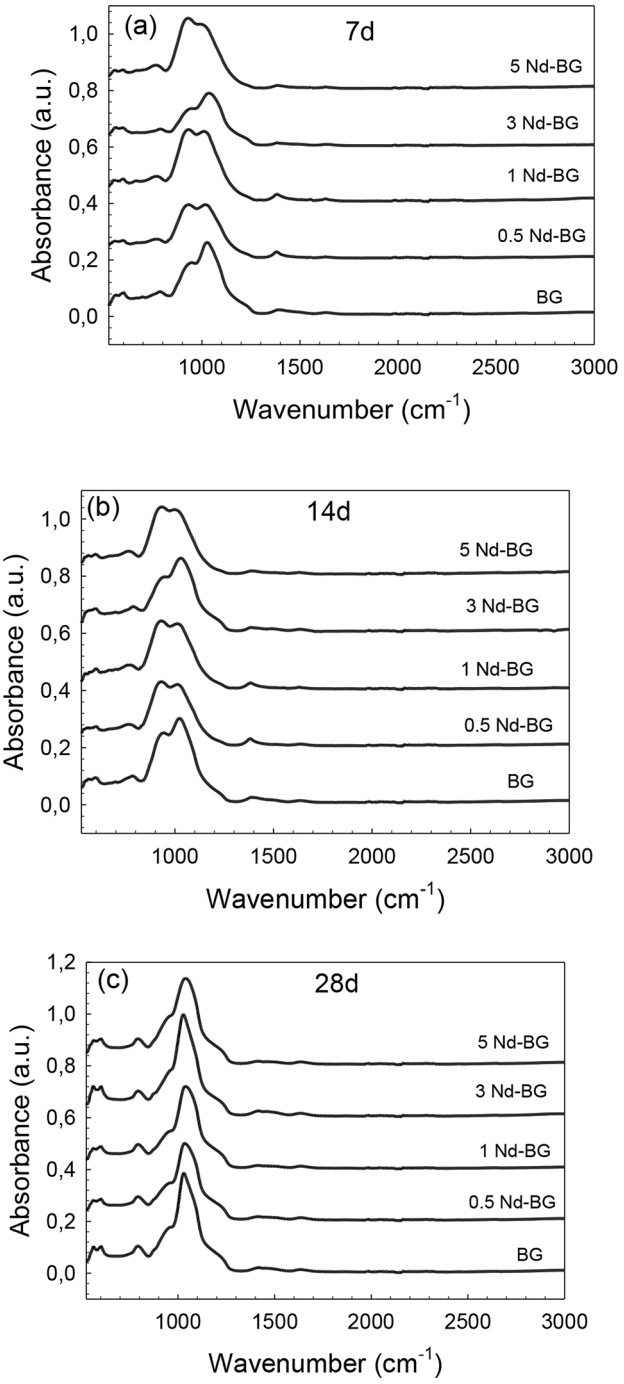

Fig. 9 FTIR spectra of the borate 13-93B3 glass particle-containing PLGA-coated 13–93 bioactive glass scaffolds immersed in SBF for (**a**) 7, (**b**) 14, and (**b**) 28 days

model, the second model that showed compatibility with the drug release behavior was the first-order model. It has been reported that the drug release kinetics from the mesoporous materials typically follows the Higuchi or the first-order model. The Higuchi model is generally used to describe drug delivery from systems having spherical morphology and other porous matrices, although the first-order model is more universal [57, 58]. Figures 13 and 14 demonstrate the Higuchi model fitting curves for the uncoated and 13-93B3 borate glass particle-containing PLGA-coated silicate-based 13–93 scaffolds. Regression coefficients for the

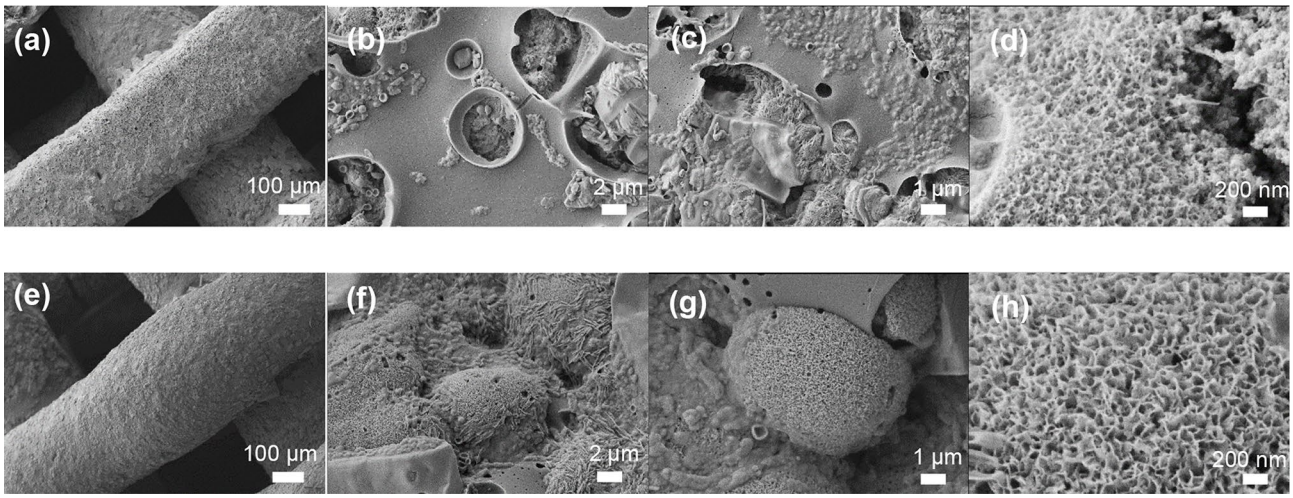

Fig. 10 SEM micrographs of the borate 13-93B3 glass particle-containing PLGA-coated 13–93 bioactive glass scaffolds immersed in SBF for 28 days (**a**)-(**d**) 0.5Nd-BG, (**e**)-(**h**) 5Nd-BG

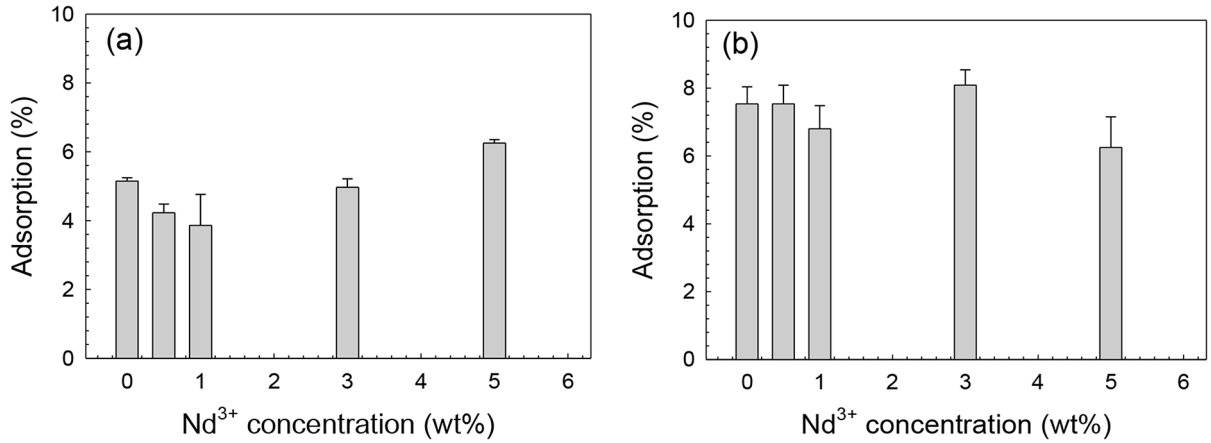

Fig. 11 Graphs showing the drug adsorption percentages of the Nd^{3+}-doped 13–93 bioactive glass scaffolds (**a**) uncoated and (**b**) borate 13-93B3 glass-containing PLGA-coated

polymer-coated glass samples were higher compared to the uncoated neat glass scaffolds.

4 Conclusions

Neodymium (III)-containing silicate-based 13–93 bioactive glass tissue engineering assemblies were fabricated using an extrusion-based robocasting technique and sol-gel-derived bioactive glass particles. The surface of the manufactured bioactive glass three-dimensional porous constructs was coated by a biopolymer (PLGA) layer containing melt-derived borate 13-93B3 bioactive glass particles. By this approach, two different types of bioactive glass compositions were utilized in the same scaffold design. The structural, morphological, mechanical characteristics and bioactivity of the prepared bioactive glass-based composite scaffolds were investigated in detail. Additionally, an antibiotic (amoxicillin) adsorption and delivery behavior of the scaffolds was examined over a period. Results showed that the PLGA coating improved the compressive strength of the glass scaffolds. All of the fabricated bioactive glass scaffolds have high bioactivity in SBF however HA formation rates were higher for the borate glass containing-polymer coated samples. Similarly, the presence of borate-based bioactive glass particles and a PLGA layer on the surface of the silicate glass scaffolds improved the drug adsorption and the release rates. Results also revealed that the presence of Nd^{3+} was not detrimental in bioactivity up to 3wt%, and increasing the drug release percentages. It was concluded that prepared scaffolds may find applications especially in bone tissue engineering by combining the mechanical strength of the silicate glass and the high reactivity (bioactivity) of borate glass in physiological fluids. Additionally,

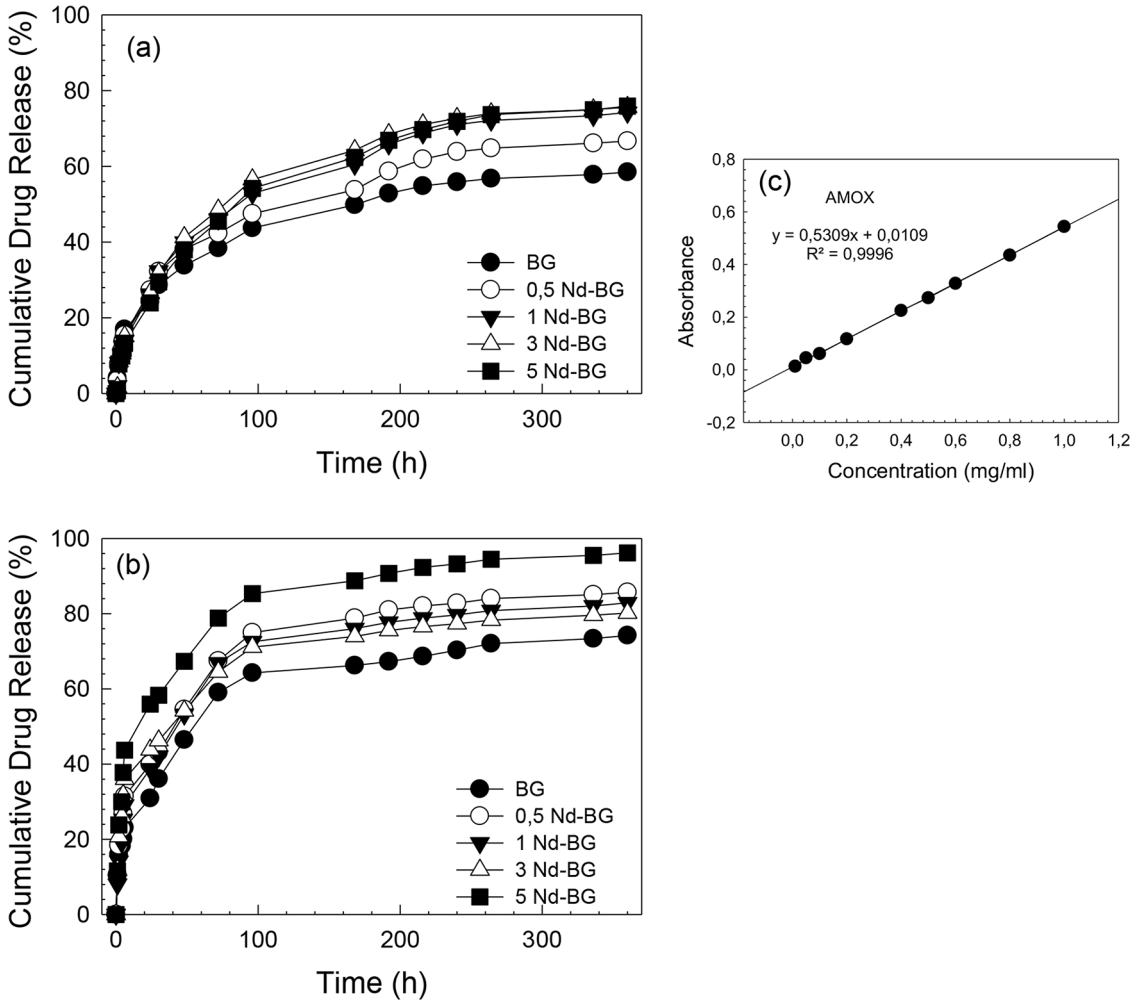

Fig. 12 Graphs showing the cumulative drug release percentages of the Nd^{3+}-doped 13–93 bioactive glass scaffolds to the PBS medium at pH 7.4 (**a**) uncoated and (**b**) borate 13-93B3 glass-containing PLGA-coated; (**c**) calibration curve for the aqueous drug solution

Table 2 Drug release kinetic model parameters for the uncoated Nd^{3+}-containing bioactive glass scaffolds. R: coefficient of correlation; K_0, K_1, K_H and K_{KP} : zero-order, first-order, Higuchi, and Korsmayer-Peppas model rate constants, respectively

Nd-BG	Zero-order		First-order		Higuchi		Korsmayer-Peppas	
	K_0	R^2	K_1	R^2	K_H	R^2	K_{KP}	R^2
BG	0.8669	0.7613	0.9899	0.7944	4.6105	0.9759	1.1488	0.7812
0.5 Nd-BG	1.0012	0.8489	0.9881	0.8856	5.6828	0.9920	1.1795	0.8050
1 Nd-BG	0.9757	0.8593	0.9885	0.8940	5.9255	0.9906	1.2764	0.8167
3 Nd-BG	0.9861	0.8309	0.9883	0.8689	6.0080	0.9871	1.3704	0.8035
5 Nd-BG	0.8929	0.8246	0.9896	0.8599	5.5428	0.9851	1.4363	0.8180

Table 3 Drug release kinetic model parameters for the coated Nd^{3+}-containing bioactive glass scaffolds. R: coefficient of correlation; K_0, K_1, K_H and K_{KP} : zero-order, first-order, Higuchi and Korsmayer-Peppas model rate constants, respectively

Nd-BG@ (PLGA + B3)	Zero-order		First-order		Higuchi		Korsmayer-Peppas	
	K_0	R^2	K_1	R^2	K_H	R^2	K_{KP}	R^2
BG	1.1384	0.7303	0.9799	0.8550	8.6042	0.9245	1.2847	0.7591
0.5 Nd-BG	0.8984	0.7934	0.9864	0.8771	7.1490	0.9610	1.1652	0.7472
1 Nd-BG	0.9276	0.8256	0.9863	0.8974	7.3401	0.9717	1.1455	0.7841
3 Nd-BG	0.8680	0.7071	0.9867	0.8036	6.7448	0.9190	1.2117	0.7412
5 Nd-BG	0.7617	0.8501	0.9894	0.9080	5.8767	0.9788	1.0498	0.7076

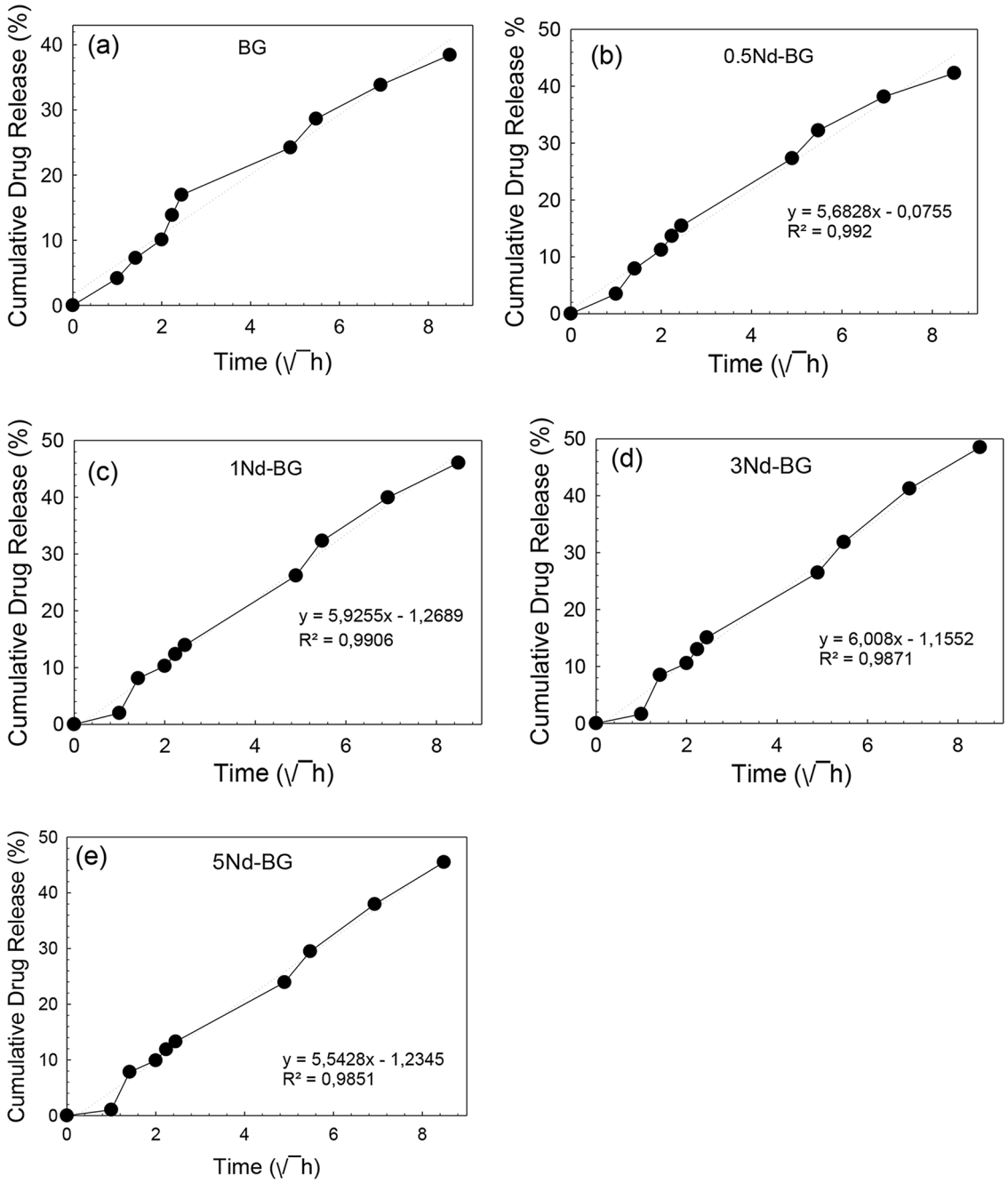

Fig. 13 Graphs showing the drug release from uncoated (**a**) bare, (**b**) 0.5 Nd^{3+}, (**c**) 1Nd^{3+}, (**d**) 3Nd^{3+}, (**e**) 5Nd^{3+}-containing silicate 13–93 bioactive glass scaffolds fitted using Higuchi kinetic model

the presence of Nd^{3+} ions in the bioactive glass matrix may be beneficial for the use of the fabricated scaffolds in photothermal therapy applications.

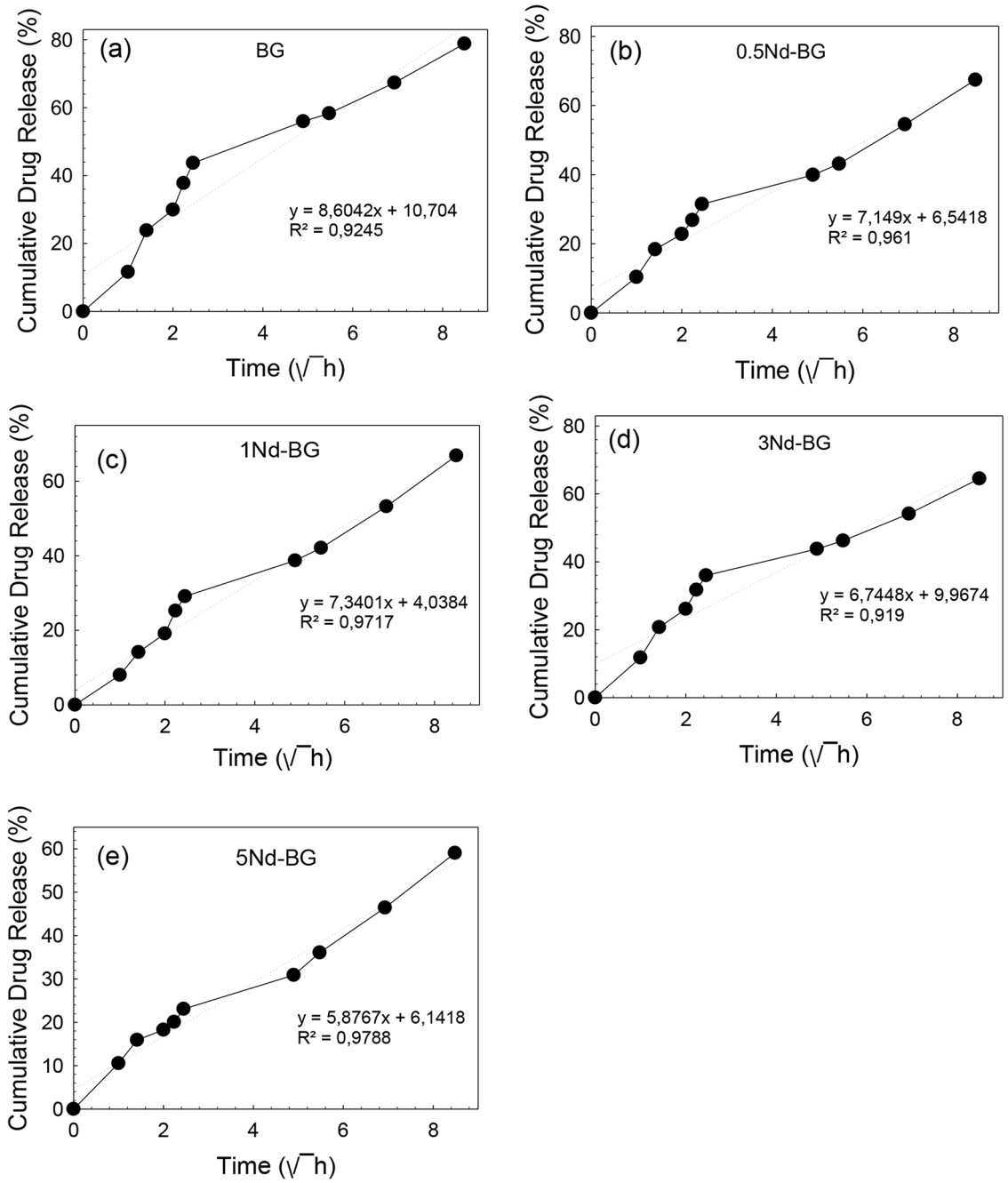

Fig. 14 Graphs showing the drug release from 13-93B3 incorporated PLGA-coated (**a**) bare, (**b**) 0.5 Nd^{3+}, (**c**) 1Nd^{3+}, (**d**) 3Nd^{3+}, (**e**) 5Nd^{3+}-containing silicate 13–93 bioactive glass scaffolds fitted using Higuchi kinetic model

Acknowledgements The financial support (MCBU-BAP project no: 2023-017) provided by the Manisa Celal Bayar University, Scientific Research Project Coordination Office was greatly acknowledged.

Authors contributions [Aylin Deliormanlı]: Conceptualization, Methodology, Investigation, Funding acquisition, Writing - Original Draft, Project administration.

Funding Open access funding provided by the Scientific and Technological Research Council of Türkiye (TÜBİTAK).

Data availability The datasets generated during and/or analyzed throughout the current study are available from the corresponding author upon request.

Declarations

Competing interest The author declares that there are no known competing financial interests or personal relationships that could have appeared to influence the work reported in this paper.

Open Access This article is licensed under a Creative Commons Attribution 4.0 International License, which permits use, sharing, adaptation, distribution and reproduction in any medium or format, as long as you give appropriate credit to the original author(s) and the source, provide a link to the Creative Commons licence, and indicate if changes were made. The images or other third party material in this article are included in the article's Creative Commons licence, unless indicated otherwise in a credit line to the material. If material is not included in the article's Creative Commons licence and your intended use is not permitted by statutory regulation or exceeds the permitted use, you will need to obtain permission directly from the copyright holder. To view a copy of this licence, visit http://creativecommons.org/licenses/by/4.0/.

References

1. L.L. Hench, R.J. Splinter, W.C. Allen, T.K. Greenlee, Bonding mechanism at the interface of ceramic prosthetic materials. J. Biomed. Mater. Res. **2**, 117–141 (1971). https://doi.org/10.1002/jbm.820050611
2. L.L. Hench, The story of bioglass®. J. Mater. Sci. Mater. Med. **17**, 967–978 (2006). https://doi.org/10.1007/s10856-006-0432-z
3. J.R. Jones, Review of bioactive glass: from Hench to hybrids. Acta Biomater. **9**(1), 4457–4486 (2013). https://doi.org/10.1016/j.actbio.2012.08.023
4. M.N. Rahaman, D.E. Day, B.S. Bal, Q. Fu, S.B. Jung, L.F. Bonewald, A.P. Tomsia, Bioactive glass in tissue engineering. Acta Biomater. **7**(6), 2355–2373 (2011). https://doi.org/10.1016/j.actbio.2011.03.016
5. A. Hoppe, N.S. Güldal, A.R. Boccaccini, A review of the biological response to ionic dissolution products from bioactive glasses and glass-ceramics. Biomaterials. **32**, 2757–2774 (2011). https://doi.org/10.1016/j.biomaterials.2011.01.004
6. B.A.E. Ben-Arfa, I.E. Palamá, I.M. Miranda Salvado, J.M.F. Ferreira, R.C. Pullar, Cytotoxicity and bioactivity assessments for Cu^{2+} and La^{3+} doped high-silica sol-gel derived bioglasses: the complex interplay between additive ions revealed. J. Biomed. Mater. Res. **107A**, 2680–2693 (2019). https://doi.org/10.1002/jbm.a.36772
7. A. Baranowska, M. Kochanowicz, A. Wajda, M. Leśniak, J. Żmojda, P. Miluski, I. Zgłobicka, K.J. Kurzydłowski, D. Dorosz, Luminescence sensing method for degradation analysis of bioactive glass fibers. Sensors. **21**(6), 2054 (2021). https://doi.org/10.3390/s21062054
8. M. Wang, G. Pi, Bo. Lei, Europium Doped Monodispersed Bioactive Glass nanoparticles regulate the osteogenic differentiation of human marrow mesenchymal stem cells. J. Biomed. Nanotechnol. **14**, 756–764 (2018). https://doi.org/10.1166/jbn.2018.2504
9. A.M. Deliormanlı, S.A.M. Issa, M.S. Al-Buriahi et al., Erbium (III)- and terbium (III)-containing silicate-based bioactive glass powders: physical, structural and nuclear radiation shielding characteristics. Appl. Phys. A **127**, 463 (2021). https://doi.org/10.1007/s00339-021-04615-5
10. A.M. Deliormanlı, R. Konyalı, Bioactive glass/hydroxyapatite-containing electrospun poly (ε-Caprolactone) composite nanofibers for bone tissue engineering. J. Aust Ceram. Soc. **55**, 247–256 (2019). https://doi.org/10.1007/s41779-018-0229-9
11. A.M. Deliormanlı, B. Rahman, S. Oğuzlar, M. Zeyrek, Ongun, Investigation of the structural, photoluminescence properties, bioactivity and 5-fluorouracil delivery behavior of Dy^{3+} and $Dy:Eu^{3+}$-doped bioactive glasses. J. Alloys Compd. **944**, 169153 (2023). https://doi.org/10.1016/j.jallcom.2023.169153
12. A.M. Deliormanlı, S. Oğuzlar, M. Zeyrek Ongun, Effects of Eu^{3+}, Gd^{3+} and Yb^{3+} substitution on the structural, photoluminescence, and decay properties of silicate-based bioactive glass powders. J. Mater. Res. **37**, 622–635 (2022). https://doi.org/10.1557/s43578-021-00461-6
13. A.M. Deliormanlı, S. Oguzlar, K. Ertekin, Photoluminescence and decay characteristics of cerium, gallium and vanadium - containing borate-based bioactive glass powders for bioimaging applications. Ceram. Int. **47**(3), 3797–3807 (2021). https://doi.org/10.1016/j.ceramint.2020.09.237
14. J.H.L. Voncken, The Rare Earth elements: an introduction. Springer Cham. **127**, 2191–5369 (2016). https://doi.org/10.1007/978-3-319-26809-5
15. B. del Rosal, U. Rocha, E.C. Ximendes, E. Martín Rodríguez, D. Jaque, García Solé, Nd^{3+} ions in nanomedicine: perspectives and applications. Opt. Mater. **63**, 185–196 (2017). https://doi.org/10.1016/j.optmat.2016.06.004
16. U. Rocha, K.U. Kumar, C. Jacinto, I. Villa, F. Sanz-Rodríguez, M. del Carmen Iglesias de la Cruz, A. Juarranz, E. Carrasco, F.C.J.M. van Veggel, E. Bovero, J.G. Solé, D. Jaque, Neodymium-doped LaF_3 nanoparticles for fluorescence bioimaging in the second biological window. Small. **10**, 1141–1154 (2014). https://doi.org/10.1002/smll.201301716
17. X. Wang, Q. Liu, Y. Bu, C.-S. Liu, T. Liu, X. Yan, Optical temperature sensing of rare-earth ion doped phosphors. RSC Adv. **5**, 86219–86236 (2015). https://doi.org/10.1039/C5RA16986K
18. S. K.Semwal, Bhatt, Study of Nd^{3+} ion as a Dopant in YAG and Glass Laser. Int. J. Phys. **1**, 15–21 (2013)
19. A. Bednarkiewicz, D. Wawrzynczyk, M. Nyk, W. Strek, Optically stimulated heating using Nd^{3+} doped NaYF4 colloidal near infrared nanophosphors. Appl. Phys. B **103**, 847–852 (2011). https://doi.org/10.1007/s00340-010-4300-7
20. S.A. de Oliveira, R. Borges, D. Dos Santos Rosa, A.C.S. de Souza, A.B. Seabra, F. Baino, Marchi, Strategies for cancer treatment based on photonic nanomedicine. Mater. (Basel). **14**(6), 1435 (2021). https://doi.org/10.3390/ma14061435
21. U. Rocha, K. Upendra Kumar, C. Jacinto, J. Ramiro, A.J. Caamaño, J. García Solé, Jaque, Nd^{3+} doped LaF3 nanoparticles as self-monitored photo-thermal agents. Appl. Phys. Lett. **104**, 053703 (2014). https://doi.org/10.1063/1.4862968
22. M. Quintanilla, A. Benayas, R. Naccache, F. Vetrone, Chap. 5, luminescent nanothermometry with lanthanide-doped nanoparticles, thermometry at the nanoscale: techniques and selected applications. R Soc. Chem. 124–166 (2016)
23. N.N. Yusof, S.K. Ghoshal, M.F. Omar, Modified absorption attributes of neodymium doped magnesium-zinc-sulfophosphate glass. Malaysian J. Fundamental Appl. Sci. **13**(3), 258–262 (2017). https://doi.org/10.11113/mjfas.v13n3.561
24. Z. Yu, Y. He, T. Schomann, K. Wu, Y. Hao, E. Suidgeest, H. Zhang, C. Eich, L.J. Cruz, Rare-earth-metal (Nd^{3+}, Ce^{3+} and Gd^{3+})-doped CaF_2: nanoparticles for multimodal imaging in biomedical applications. Pharmaceutics. **14**(12), 2796 (2022). https://doi.org/10.3390/pharmaceutics14122796
25. S. Rehman, M.A. Ansari, M.A. Alzohairy, M.N. Alomary, B.R. Jermy, R. Shahzad, N. Tashkandi, Z.H. Alsalem, Antibacterial and antifungal activity of novel synthesized neodymium-substituted cobalt ferrite nanoparticles for biomedical applications. Processes. **7**(10), 714 (2019). https://doi.org/10.3390/pr7100714
26. S.M. El-Bashir, Physical properties Nd^{3+} doped (SiO_2–TiO_2) monolithic glass for photoresistor applications. Mater. Res. Express. **4**(11), 115203 (2017). https://doi.org/10.1088/2053-1591/aa97a7
27. L. Ma, Y. Zhou, Z. Zhang, Y. Liu, D. Zhai, H. Zhuang, Q. Li, J. Yuye, C. Wu, J. Chang, Multifunctional bioactive Nd-Ca-Si glasses for fluorescence thermometry, photothermal therapy, and burn tissue repair. Sci. Adv. **6**, 32 (2020). https://doi.org/10.1126/sciadv.abb1311

28. A.M. Deliormanlı, A.M. Yıldırım, Sol-gel synthesis of 13–93 bioactive glass powders containing therapeutic agents. J. Aust Ceram. Soc. **52**(2), 9–19 (2016)
29. A.M. Deliormanlı, M. Türk, Flow behavior and drug release study of injectable Pluronic F-127 hydrogels containing bioactive glass and carbon-based nanopowders. J. Inorg. Organomet. Polym. **30**, 1184–1196 (2020). https://doi.org/10.1007/s10904-019-01346-2
30. A. Sakar-Deliormanlı, E. Çelik, M. Polat, Adsorption of anionic polyelectrolyte and comb polymers onto lead magnesium niobate. Colloids Surf. A, **316**(1–3), 202–209 (2008). https://doi.org/10.1016/j.colsurfa.2007.09.004
31. T. Kokubo, H. Takadama, How useful is SBF in predicting in vivo bone bioactivity? Biomaterials. **27**(15), 2907–2915 (2006). https://doi.org/10.1016/j.biomaterials.2006.01.017
32. T. Yao, Y. Asayama, Animal-cell culture media: history, characteristics, and current issues. Reprod. Med. Biol. **16**(2), 99–117 (2017). https://doi.org/10.1002/rmb2.12024
33. G. Binson, C. Grignon, G. Le Moal, P. Lazaro, J. Lelong, F. Roblot et al., Overcoming stability challenges during continuous intravenous administration of high-dose Amoxicillin using portable elastomeric pumps. PLoS ONE. **14**(8), e0221391 (2019). https://doi.org/10.1371/journal.pone.0221391
34. C.B. Landersdorfer, M. Kinzig, J.B. Bulitta, F.F. Hennig, U. Holzgrabe, F. Sörgel, J. Gusinde, Bone penetration of Amoxicillin and clavulanic acid evaluated by population pharmacokinetics and Monte Carlo simulation. Antimicrob. Agents Chemother. **53**(6), 2569–2578 (2009). https://doi.org/10.1128/AAC.01119-08
35. N.W. Cortés-Penfield, P.A. Kulkarni, The history of antibiotic treatment of osteomyelitis. Open. Forum Infect. Dis. **6**(5), ofz181 (2019). https://doi.org/10.1093/ofid/ofz181
36. R. Karaman, in From conventinal prodrugs to prodrugs designed by molecular orbital methods, ed. by Zaheer-ul-Haq, J. D. Madura. Frontiers in Computational Chemistry, Chapter 5 (Bentham Science Publishers, 2015), pp. 187–249. https://doi.org/10.2174/9781608059782115020007
37. M. Luciano Bruschi, 5 - Mathematical models of drug release, strategies to modify the drug release from pharmaceutical systems,Woodhead Publishing, 63–86 (2015), https://doi.org/10.1016/B978-0-08-100092-2.00005-9
38. C.C. Zhang, X. Gao, B. Yilmaz, Development of FTIR spectroscopy methodology for characterization of boron species in FCC catalysts. Catalysts. **10**(11), 1327 (2020). https://doi.org/10.3390/catal10111327
39. A.M. Deliormanlı, H. Atmaca, Effect of pore architecture on the mesenchymal stem cell responses to graphene/polycaprolactone scaffolds prepared by solvent casting and robocasting. J. Porous Mater. **27**, 49–61 (2020). https://doi.org/10.1007/s10934-019-00791-1
40. A.M. Efimov, V.G. Pogareva, IR absorption spectra of vitreous silica and silicate glasses: the nature of bands in the 1300 to 5000 cm^{-1} region. Chem. Geol. **229**, 198–217 (2006). https://doi.org/10.1016/j.chemgeo.2006.01.022
41. W.R. Taylor, Application of infrared spectroscopy to studies of silicate glass structure: Examples from the melilite glasses and the systems Na_2O-SiO_2 and Na_2O-Al_2O_3-SiO_2, Proc. Indian Acad. Sci. (Earth Planet. Sci.), 99(1), 99–117 (1990)
42. M. Trivedi, A. Branton, D. Trivedi, G. Nayak, K. Bairwa, Spectroscopic characterization of disodium hydrogen orthophosphate and sodium nitrate after biofield treatment. J. Chromatogr. Sep. Tech. **6**(5), 282 (2015). https://doi.org/10.4172/2157-7064.1000282
43. C.E. Misch, Z. Qu, M.W. Bidez, Mechanical properties of trabecular bone in the human mandible: implications for dental implant treatment planning and surgical placement. J. Oral Maxillofac. Surg. **57**(6), 700–708 (1999). https://doi.org/10.1016/s0278-2391(99)90437-8
44. L. Zhao, C. Wu, K. Lin, J. Chang, The effect of poly(lactic-co-glycolic acid) (PLGA) coating on the mechanical, biodegradable, bioactive properties and drug release of porous calcium silicate scaffolds. Biomed. Mater. Eng. **22**, 289–300 (2012). https://doi.org/10.3233/BME-2012-0719
45. A.M. Deliormanlı, M. Ensoylu, G. ALMisned, H.O. Tekin, Two-dimensional molybdenum disulfide/polymer-coated bioactive glass scaffolds for tissue engineering: Fabrication, structural, mechanical, bioactivity, and radiation interaction properties. Ceram Int. **49**, Part A, 22861–22874 (2023). https://doi.org/10.1016/j.ceramint.2023.04.110
46. Y. Kang, A. Scully, D.A. Young, S. Kim, H. Tsao, M. Sen, Y. Yang, Enhanced mechanical performance and biological evaluation of a PLGA coated β-TCP composite scaffold for load-bearing applications. Eur. Polym. J. **47**(8), 1569–1577 (2011). https://doi.org/10.1016/j.eurpolymj.2011.05.004
47. O.H. Andersson, K.H. Karlsson, K. Kangasniemi, Calcium phosphate formation at the surface of bioactive glass in vivo. J. Non Cryst. Solids. **119**, 290–296 (1990). https://doi.org/10.1016/0022-3093(90)90301-2
48. G.A. Stanciu, I. Sandulescu, B. Savu, S.G. Stanciu, K.M. Paraskevopoulos et al., Investigation of the Hydroxyapatite Growth on Bioactive Glass Surface. J. Biomedical Pharm. Eng. **1**(1), 34–39 (2007)
49. L. Berzina-Cimdina, N. Borodajenko, Research of Calcium Phosphates Using Fourier Transform Infrared Spectroscopy, Infrared Spectroscopy - Materials Science, Engineering and Technology, Theophanides Theophile (Ed.), 2012, ISBN: 978-953-51-0537-4
50. A. Nommeots-Nomm, L. Hupa, D. Rohanová, D.S. Brauer, A review of acellular immersion tests on bioactive glasses—influence of medium on ion release and apatite formation. Int. J. Appl. Glass Sci. **11**, 537–551 (2020). https://doi.org/10.1111/ijag.15006
51. P. Sepulveda, J.R. Jones, L.L. Hench, In vitro dissolution of melt-derived 45S5 and sol-gel derived 58S bioactive glasses. J. Biomed. Mater. Res. **61**(2), 301–311 (2002). https://doi.org/10.1002/jbm.10207
52. G. Lopes da Silva, I.F. Rodrigues, S.S. Silva Pereira, G.M. Gomes Fontoura, A. Silva Reis, F. Pedrochi, A. Steimacher, Bioactive antibacterial borate glass and glass-ceramics. J. Non-cryst. Solids. **595**, 121829 (2022). https://doi.org/10.1016/j.jnoncrysol.2022.121829
53. R.F. Brown, M.N. Rahaman, A.B. Dwilewicz, W. Huang, D.E. Day, Y. Li, B.S. Bal, Effect of borate glass composition on its conversion to hydroxyapatite and on the proliferation of MC3T3-E1 cells. J. Biomed. Mater. Res. Part. A **88**, 392–400 (2009). https://doi.org/10.1002/jbm.a.31679
54. Z. Zhuang, H. Yamamoto, M. Aizawa, Synthesis of plate-shaped hydroxyapatite via an enzyme reaction of urea with urease and its characterization. Powder Technol. **222**, 193–200 (2012). https://doi.org/10.1016/j.powtec.2012.02.046
55. A. Doostmohammadi, A. Monshi, R. Salehi, M.H. Fathi, Z. Golniya, A.U. Daniels, Bioactive glass nanoparticles with negative zeta potential. Ceram. Int. **37**, 2311–2316 (2011). https://doi.org/10.1016/j.ceramint.2011.03.026
56. Z. Tabiaa, K. El Mabrouk, M. Bricha, K. Nouneh, Mesoporous bioactive glass nanoparticles doped with magnesium: drug delivery and acellular in vitro bioactivity. RSC Adv. **9**, 12232–12246 (2019). https://doi.org/10.1039/C9RA01133A
57. E. Beňová, D. Bergé-Lefranc, V. Zeleňák, M. Almáši, V. Huntosova, V. Hornebecq, Adsorption properties, the pH-sensitive release of 5-fluorouracil and cytotoxicity studies of mesoporous silica drug delivery matrix. Appl. Surf. Sci. **504**, 144028 (2021). https://doi.org/10.1016/j.apsusc.2019.144028
58. L. Polo, N. Gómez-Cerezo, A. García-Fernández, E. Aznar, J.-L. Vivancos, D. Arcos, M. Vallet-Regí, R. Martínez-Máñez, Mesoporous bioactive glasses equipped with stimuli-responsive

molecular gates for controlled delivery of levofloxacin against bacteria. Chem. - Eur. J. **24**, 18944 (2018). https://doi.org/10.1002/chem.201803301

Publisher's Note Springer Nature remains neutral with regard to jurisdictional claims in published maps and institutional affiliations.